CHINESE OPTICS LETTERS

Vol. 21, No. 8 | August 2023

Spatiotemporal optical vortex wavepackets with phase singularities embedded in multiple domains [Invited]

Liangliang Gu (顾亮亮)[1,2], Qian Cao (曹 前)[1,2*], and Qiwen Zhan (詹其文)[1,2]

[1] School of Optical-Electrical and Computer Engineering, University of Shanghai for Science and Technology, Shanghai 200093, China

[2] Zhangjiang Laboratory, Shanghai 201204, China

*Corresponding author: cao.qian@usst.edu.cn

Received March 31, 2023 | Accepted May 18, 2023 | Posted Online August 7, 2023

Spatiotemporal optical vortex (STOV) wavepacket carrying transverse photonic orbital angular momentum (OAM) has been extensively studied in the past few years. In this Letter, we propose and study a novel STOV wavepacket with multiple phase singularities embedded in different space–time domains using analytical and numerical approaches. By tuning different parameters used for designing the wavepacket, it is possible to engineer both the magnitude and orientation of the photonic OAM in space–time. The vectorially controllable OAM will pave new avenues and facilitate applications such as novel optical communication, studying complicated quantum systems, and spin-and-OAM interactions.

Keywords: spatiotemporal optical vortices; photonic orbital angular momentum; ultrafast optics.

DOI: 10.3788/COL202321.080003

1. Introduction

In the past few years, the interest in studying spatiotemporal coupled (STc) optical fields is growing rapidly. Compared with conventional spatiotemporal uncoupled optical fields, STc fields have a much more complicated field distribution in space–time, allowing the field to possess unique and interesting property such as propagating without spreading in space–time[1–3], having a spring-like spatiotemporal structure[4], propagating in an arbitrary group velocity[5], and carrying photons with transverse photonic orbital angular momentum (OAM)[6,7].

Among these studies, spatiotemporal optical vortex (STOV) wavepacket carrying transverse OAM is one of the most interesting research topics and has drawn the most attention. In the past three decades, the photonic research community has been following the path in studying optical fields with a longitudinal OAM. In 1992, Allen discovered that an optical vortex beam with a spiral phase front of $\exp(il\theta_{xy})$ can carry a photon with a longitudinal OAM[8]. For such a vortex beam, the orientation of the OAM is parallel to the direction in which light propagates. With this property, the vortex beam has enabled numerous applications, including optical manipulation[9], optical communication[10], quantum optics[11], and many others[12]. On the other hand, very few research works have focused on studying optical field carrying transverse OAM. It has been proposed that the light field can carry transverse OAM in the form of polychromatic STOV pulses[13,14]. In 2016, the first experimental demonstration of generating STOV pulses was presented[15]. In the experiment, the STOV pulse was generated by self-focusing an intense laser pulse in a nonlinear pulse propagation process. The generated STOV pulse only has a portion of the total pulse energy, and the process lacks control over the pulse. Later, research groups have found that a STOV pulse can be generated by using a two-dimensional (2D) phase modulation device placed in the spatial–spectral (x–ω) plane[6,7]. The generated STOV pulse can have a controllable spiral phase of $\exp(il\theta_{xt})$ in the spatiotemporal domain, and the photon within the pulse carries transverse OAM of $l\hbar$ per photon. After that, many research works have studied the propagation dynamics of STOV pulses[16,17], conservation of OAM during frequency conversion processes[18,19], generating nonspreading STOV wavepackets[20,21], generating STOV pulses from a partially coherent source[22], developing novel characterization methods[23–25], using STOV pulses to detect sharp changes of pulse envelopes[26], and synthesizing even more exotic wavepackets that also carry transverse OAM[27].

Despite the amount of work that has been accomplished after scientists elucidated how to generate STOV pulses controllably, very few were studying wavepackets with multiple phase singularities[28–30]. Wan *et al.* studied, both analytically and experimentally, a STOV wavepacket with its phase singularity located in the x–z plane intersecting with another phase singularity in the x–y plane[29]. Such a wavepacket can carry a photon with an OAM orientated in the y–z plane. The orientation of the OAM can stay in the y–z plane as the wavepacket propagates. However, in general, the orientation of photonic OAM is vectorial, meaning it can be freely tuned in any direction in the three-dimensional space–time. The realization of a full-vectorial

photonic OAM will bring new opportunities in many new applications, such as utilizing the wavepacket for manipulating complicated quantum systems, using vectorial OAM as a carrier for optical communication, and performing spin-OAM interaction studies.

In this paper, we propose and theoretically study a novel STOV wavepacket with phase singularities embedded in multiple space–time domains. We study two types of STOV wavepacket, with a particular emphasis on the second one. Both types of STOV wavepackets have the capability of tuning the magnitude and the orientation of the transverse OAM by changing the parameters that define the wavepacket. In the first type, phase singularities are embedded in the x–z and y–z domains with varying scaling factors. Using analytical approaches, we show that by varying the scaling factor of the spiral phase in the x, y, and z directions, it is possible to tune the magnitude and orientation of the transverse OAM continuously. However, to achieve a wider tuning range for the orientation, the OAM's magnitude is compromised, and, therefore, we propose the second type of STOV wavepacket by placing multiple phase singularities in the x–z and x'–z planes. Here, the x' axis is in the x–y plane with an angle difference of $\theta_{x-x'}$ with respect to the x axis. For such a wavepacket, the transverse OAM can be continuously tuned by controlling $\theta_{x-x'}$, and the resulting transverse OAM has a wider tuning range for its orientation without compromising its magnitude. Combining such a wavepacket with an additional phase singularity in the x–y plane, it is possible to generate a wavepacket carrying full-vectorial photonic OAM in an all space–time domain. Such a wavepacket may facilitate applications such as novel optical communication and studying complicated quantum systems.

2. Results and Discussions

We first use an analytical approach to study STOV wavepackets with multiple phase singularities placed in different space–time domains. Before we officially start the study, we list here some essential equations used for this part of the study. We assume a wavepacket polarized in the x direction is propagating in the z direction with a vector potential of $\boldsymbol{A}$. The potential $\boldsymbol{A}$ can be written as

$$\boldsymbol{A} = \hat{\boldsymbol{x}} \cdot u(x, y, z) e^{-ikz}, \tag{1}$$

where $\hat{\boldsymbol{x}}$ is the unit vector in the x direction, $u(x, y, z)$ is the complex scalar function for describing the field in the paraxial regime, and k is the propagation constant. With this expression, the linear momentum density of the wavepacket can be expressed by[8,31]

$$\boldsymbol{g} = i\omega \frac{\epsilon_0}{2} (u^* \nabla u - u \nabla u^*) + \omega k \epsilon_0 |u|^2 \hat{\boldsymbol{z}}, \tag{2}$$

where $\nabla = \hat{\boldsymbol{x}} \frac{\partial}{\partial x} + \hat{\boldsymbol{y}} \frac{\partial}{\partial y} + \hat{\boldsymbol{z}} \frac{\partial}{\partial z}$. The angular momentum density $\boldsymbol{p}$ can be expressed by the cross product between the position vector $\boldsymbol{r}$ and the linear momentum density vector $\boldsymbol{g}$, written as

$$\boldsymbol{p} = \boldsymbol{r} \times \boldsymbol{g}. \tag{3}$$

The average photonic OAM per photon within the wavepacket can be then calculated by the volume integral, written as

$$\text{OAM/photon} = \frac{\int_{-\infty}^{\infty} \boldsymbol{r} \times \boldsymbol{g} \, \mathrm{d}V}{\epsilon_0 \omega^2 \int_{-\infty}^{\infty} |u|^2 \, \mathrm{d}V} \hbar\omega. \tag{4}$$

With these equations, we now start to study an x-polarized wavepacket with two phase singularities embedded in the x–z plane and y–z plane, respectively. It is noteworthy that the field distribution of such a wavepacket cannot be decomposed into spatiotemporal fields that are located in a 2D + 1D fashion[16] as the wavepacket is now three-dimensionally coupled. The field can be written as

$$u(x, y, z) = \left(\frac{x}{w_x} + i \cdot \mathrm{Sgn}(l_1) \frac{z}{w_z} \right)^{|l_1|} \left(\frac{y}{w_y} + i \cdot \mathrm{Sgn}(l_2) \frac{z}{w_z} \right)^{|l_2|}, \tag{5}$$

where l_1 is the topological charge for the spiral phase in x–z and l_2 is the topological charge in y–z. w_x, w_y, and w_z are the scaling factors of the applied spatiotemporal phase in the x, y, and z directions. $\mathrm{Sgn}(x)$ is the sign function. By putting Eq. (5) into Eqs. (2)–(4) and setting both l_1 and l_2 equal to 1, we can get the average OAM within the wavepacket equal to

$$\text{OAM/photon} = \hbar \left(\frac{-2 w_y w_z (7 w_x^2 + 5 w_z^2)}{5(w_z^4 + w_x^2 w_z^2 + w_y^2 w_z^2) + 9 w_x^2 w_y^2}, \frac{2 w_x w_z (7 w_y^2 + 5 w_z^2)}{5(w_z^4 + w_x^2 w_z^2 + w_y^2 w_z^2) + 9 w_x^2 w_y^2}, 0 \right). \tag{6}$$

The expression shown in the bracket stands for the magnitude of the OAM vector in the x, y, and z directions. The result is obtained by using the Mathematica program to perform the numerical integral calculation. Since the STOV wavepacket only has a spiral phase in the x–z plane and y–z plane, the OAM carried by the wavepacket has a zero component in the z direction, and the orientation of the OAM is always in the x–y plane.

At the state where the applied spatiotemporal phase has the same scaling factor $w_x = w_y = w_z$, the wavepacket carries transverse OAM equal to $(-\hbar, \hbar, 0)$. The magnitude of this OAM is $\sqrt{2}\hbar$, and the OAM points at 135° in the x–y plane. Figure 1 shows the change of the transverse OAM when the scaling factor w_z is fixed at 1 while both w_x and w_y are varying. In Fig. 1(a1), w_y is fixed at 1 and w_x changes from 0.2 to 5. In such a case, the OAM projection in the x direction has no change, as it is related to the spiral phase structure in the y–z plane. Meanwhile, the OAM projection in the y direction, OAM_y, reaches a maximum magnitude of around $1.01\hbar$ when w_x is 0.845. A similar trend is found in Fig. 1(a2) for the case when the wavepacket has a fixed

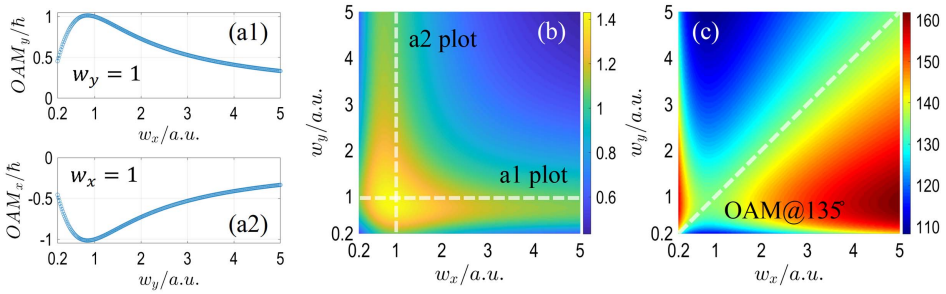

Fig. 1. OAM of STOV wavepacket with phase singularities embedded in the x–z and y–z domains with vary scaling factors. (a) OAM projection in the y direction and x direction when w_y or w_x is fixed; (b) magnitude of OAM with changing w_x and w_y. The dashed lines correspond to results shown in (a1) and (a2). (c) Orientation of OAM in the x–y plane with varying w_x and w_y.

w_x at 1 and a varying w_y. When both w_x and w_y are changing simultaneously, the magnitude of the OAM will be changed. We plot in Fig. 1(b) the magnitude of the OAM defined as $|\mathrm{OAM}_x^2 + \mathrm{OAM}_y^2 + \mathrm{OAM}_z^2|^{1/2}$ divided by the reduced Planck constant $\hbar$ with different combinations of w_x and w_y. The magnitude of the OAM reaches a maximum value of $1.43\hbar$ when the scaling factors w_x and w_y equal 0.8776. The white dashed lines shown in Fig. 1(b) correspond to the trace plotted in Figs. 1(a1) and 1(a2). Figure 1(c) plots the orientation of the OAM in the x–y plane when the scaling factors w_x and w_y change. The direction of the OAM can be tuned from 110° to 160° as w_x or w_y changes. For the case when $w_x = w_y$ [white dashed line in Fig. 1(c)], the OAM always points at 135° in the x–y plane.

The above example shows the OAM property of the STOV wavepacket with phase singularities embedded in the $x-z$ and $y-z$ planes with different scaling factors. The magnitude of the transverse OAM can be tuned by changing the scaling factor. The orientation of the transverse OAM can be also tuned. To redirect the OAM orientation from 135° angle, w_x must be different from w_y. However, in such a case, the magnitude of the resulting OAM drops quickly. For example, in the case where $w_x = 1$ and $w_y = 4$, the OAM points at around 110° in the x–y plane, and the magnitude of the OAM drops to about $0.4\hbar$. In this case, the tuning range of the OAM direction is about 50°, from 110° to 160°, while the magnitude of the OAM can be down to $0.4\hbar$.

To engineer the transverse OAM of a STOV wavepacket with a greater tuning range in its orientation but also with less compromise in its magnitude, we propose here another possible route: placing the secondary phase singularity in a plane that has an angle with respect to the x–z plane. Let us call this plane the x'–z plane. The x' axis is set to be in the x–y plane, and it has an angle offset of $\theta_{x-x'}$ with respect to the x axis. Assuming the applied spiral phase has the same scaling factor, the wavepacket can be written as

$$u(x,y,z) = (x + i\cdot \mathrm{Sgn}(l_1)z)^{|l_1|}(x' + i\cdot \mathrm{Sgn}(l_2)z)^{|l_2|}, \quad (7)$$

where x' is defined as $x' = x\cos\theta_{x-x'} + y\sin\theta_{x-x'}$. Using Eq. (7) in Eqs. (2)–(4) and setting both l_1 and l_2 equal to 1, the average OAM within the wavepacket equals

$$\mathrm{OAM/photon} = \hbar\left(-\frac{24\sin(\theta_{x-x'}) + 5\sin(2\theta_{x-x'})}{2(13+\cos(2\theta_{x-x'}))}, \frac{4\cos^2\left(\frac{\theta_{x-x'}}{2}\right)(6+\cos\theta_{x-x'})}{13+\cos(2\theta_{x-x'})}, 0\right). \quad (8)$$

In the case where the x' axis coincides with the y axis, meaning when $\theta_{x-x'} = \pm\pi/2$, the wavepacket carries an OAM of $(\mp\hbar, \hbar, 0)$. Changing $\theta_{x-x'}$ offers a new degree of freedom for tuning both the orientation and the magnitude of the OAM. Figure 2(a) shows the change of OAM projection in the x direction [Fig. 2(a1)] and in the y direction [Fig. 2(a2)] when $\theta_{x-x'}$ changes from $-\pi$ to $+\pi$. When $\theta_{x-x'} = 0$, or when the x' axis aligns with the x axis, the OAM is $(0, 2\hbar, 0)$. When $\theta_{x-x'}$ decreases from 0 to $-\pi$, the OAM's projection in the x direction has a maximum value of $1.06\hbar$ at $\theta_{x-x'} = -0.41\pi$. Meanwhile, when $\theta_{x-x'}$ changes from 0 to $-\pi$, the OAM projection in the y direction drops from $2\hbar$ to 0.

It is noteworthy that the above analysis is based upon an analytical calculation for revealing the OAM feature of the wavepacket. This model clearly deviates from the vector model for understanding the transverse OAM in a more intuitive manner. In the vector model, the overall OAM is the superposition of an OAM of $\hbar$ in the y direction (contribution from spiral phase in the x–z plane) and another OAM of $\hbar$ in the $(\theta_{x-x'} + \pi/2)$ direction (a contribution from the spiral phase in the x'–z plane). The OAM from the vector model equals

$$\mathrm{OAM/photon} = \hbar(0,1,0) + \hbar(-\sin\theta_{x-x'}, \cos\theta_{x-x'}, 0). \quad (9)$$

Figure 2(b) shows the magnitude of the OAM carried by the wavepacket calculated by both the analytic model and the vector model. Both models have a similar trend in terms of the change of OAM magnitude with a changing $\theta_{x-x'}$, but they are marginally different. Figure 2(c) shows the vectorial representation of the transverse OAM $(\mathrm{OAM}_x, \mathrm{OAM}_y)$ in a polar coordinate plot. $\theta_{x-x'}$ changes from $-\pi$ to $+\pi$. The orientation of the transverse OAM can be tuned in a range of 90° from 45° to 135°, while the magnitude of the OAM is always larger than $1.5\hbar$.

Figure 3 shows the spatiotemporal intensity and phase profile of STOV wavepackets with two phase singularities embedded in the x–z and x'–z planes. The angle difference between the x axis

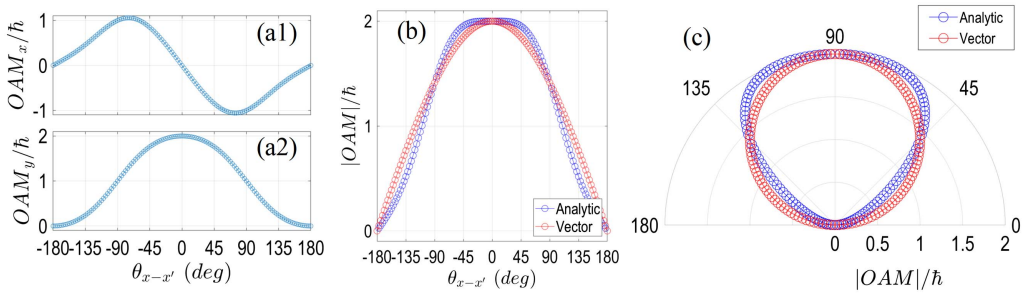

Fig. 2. OAM of STOV wavepacket with phase singularities embedded in the x–z and x'–z domains. The x' axis lies in the x–y plane with an offset angle of $\theta_{x-x'}$ with respect to the x axis. (a) Projection of OAM in the x direction and y direction when $\theta_{x-x'}$ changes; (b) magnitude of OAM using both the analytical model and the vector model; (c) vectorial representation of the transverse OAM in the x–y plane using two different models.

and x' axis is set to be $0, \pi/4, \pi/2, 3\pi/4$, and π (from left to right in Fig. 3), respectively. Figure 3(a) shows the intensity isosurface plot when the spatiotemporal intensity of the wavepacket is at 15% and 50% of the intensity maximum. All figures have shown the spatiotemporal phase singular feature of this type of wavepacket, indicated by the intensity null within the wavepacket. Figure 3(b) shows the spatiotemporal phase profile of the wavepacket plotted on the top of the isosurface plot at 15% peak intensity. All the plots have shown the spiral phase in the spatiotemporal domain except for the case where $\theta_{x-x'} = \pi$. Using Eq. (8), the OAM carried by the wavepacket is calculated to be $(0, 2\hbar, 0)$, $(-0.845\hbar, 1.761\hbar, 0)$, $(-\hbar, \hbar, 0)$, $(-0.46\hbar, 0.23\hbar, 0)$, and (0, 0, 0). Figure 3(c) shows the 15% (5% for the case where $\theta_{x-x'} = \pi/2$) intensity isosurface from an x–y plane perspective. It can be clearly seen that when $\theta_{x-x'} = \pi/4$ and $3\pi/4$, the direction of the OAM has a tilted angle with respect to the y axis.

Finally, we propose here the route for designing a STOV wavepacket with full control of the photonic OAM in three-dimensional space–time by combining the wavepacket in Eq. (7) with an additional phase singularity placed in the spatial x–y plane. The wavepacket is expressed by

$$u(x,y,z) = (x + i\cdot \mathrm{Sgn}(l_1)z)^{|l_1|}(x' + i\cdot \mathrm{Sgn}(l_2)z)^{|l_2|} \times (x + i\cdot \mathrm{Sgn}(l_3)y)^{|l_3|}, \tag{10}$$

where l_3 stands for the topological charge in the x–y plane. By setting $l_1 = l_2 = l_3 = 1$ and using Eqs. (2)–(4), we can get the averaged OAM per photon,

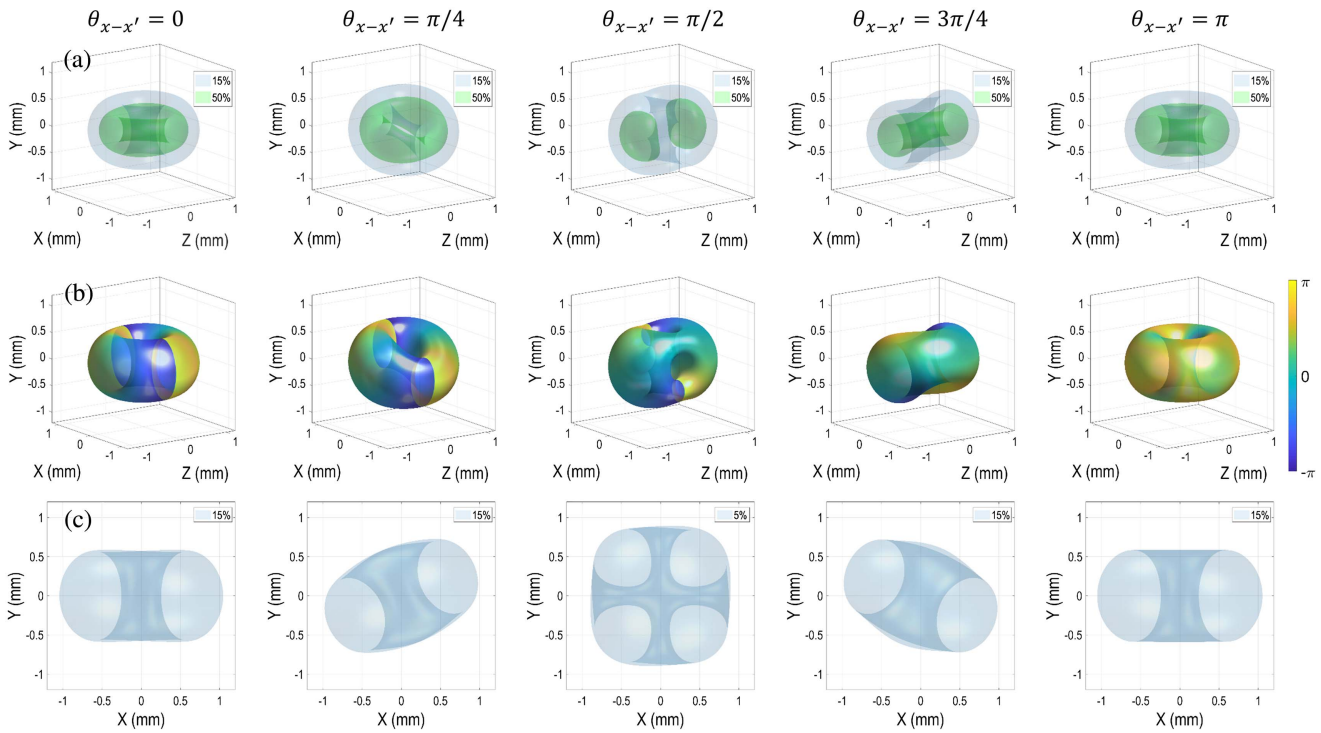

Fig. 3. Spatiotemporal intensity and phase profile of STOV wavepackets with phase singularities embedded in the x–t and x'–t domains; the angle difference between the x and x' axes changes from 0 to π in an interval of $\pi/4$ (from left to right). (a) Intensity isosurface plot at 15% and 50% of the intensity maximum; (b) phase distribution on the 15% intensity isosurface plot; (c) intensity isosurface plot (15%) in the x–y plane.

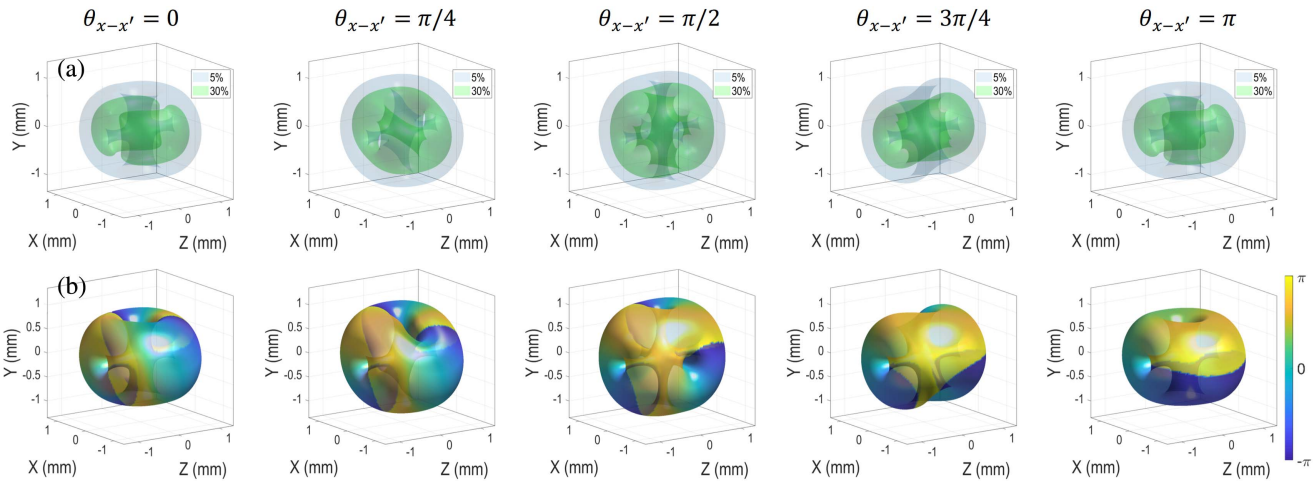

Fig. 4. Spatiotemporal intensity and phase profile of STOV wavepackets with phase singularities embedded in the x–z, x'–z, and x–y planes; $\theta_{x-x'}$ changes from 0 to π in an interval of $\pi/4$ (from left to right). (a) Intensity isosurface plot at 5% and 30% of the peak intensity; (b) phase profile on the top of 5% intensity isosurface.

$$\mathrm{OAM/photon} = \hbar\left(-\frac{224\ \sin\ (\theta_{x-x'}) + 63\ \sin\ (2\theta_{x-x'})}{2(121 + 9\ \cos\ (2\theta_{x-x'}))},\right.$$
$$\left.\frac{4\cos^2\left(\frac{\theta_{x-x'}}{2}\right)(56 + 9\ \cos\ \theta_{x-x'})}{121 + 9\ \cos\ (2\theta_{x-x'})}, -1\right). \quad (11)$$

Using Eq. (11), the magnitude |OAM|, the polar angle θ, and the azimuthal angle φ of the OAM carried by the wavepacket can be calculated. Figure 4 shows the spatiotemporal intensity and phase profile of the wavepacket when $\theta_{x-x'}$ changes from 0 to π in an interval of $\pi/4$ (from left to right). Figure 4(a) shows the intensity isosurface at 5% and 30% of the peak intensity. Note here the transverse OAM contributed by the spiral phase in the x–z and x'–z planes is always perpendicular to the longitudinal OAM contributed by the spiral phase in the x–y plane, and, therefore, the intensity null of the wavepacket does not merge together. Figure 4(b) shows the phase profile overlaying the top of the intensity isosurface at 5%. The OAM carried by the wavepacket is $(0, 2\hbar, -\hbar)$, $(-0.914\hbar, 1.760\hbar, -\hbar)$, $(-\hbar, \hbar, -\hbar)$, $(-0.394\hbar, 0.240\hbar, -\hbar)$, and $(0, 0, -\hbar)$.

3. Conclusions and Outlook

In conclusion, we studied two types of novel STOV wavepackets with multiple phase singularities embedded in different space–time domains. Both types have the capability of tuning the orientation and the magnitude of the transverse OAM carried by the wavepacket in the x–y plane, but the second type clearly has the advantage over the first one, as it allows a wider tuning range for the OAM orientation without compromising the magnitude of the OAM. Combining the second type of STOV wavepacket with a third spiral phase placed in the x–y planes allows the full-vectorial control over the photonic OAM. Such a wavepacket can bring new opportunity in new research and applications such as optical communication and studying complicated quantum systems.

Acknowledgement

This work was supported by the National Natural Science Foundation of China (NSFC) (Nos. 92050202, 12104309, and 62005168), the Shanghai Science and Technology Committee (No. 19060502500), and the Shanghai Sailing Program (No. 21YF1431500).

References

1. Y. Silberberg, "Collapse of optical pulses," Opt. Lett. **15**, 1282 (1990).
2. H. Sõnajalg, M. Rätsep, and P. Saari, "Demonstration of the Bessel-X pulse propagating with strong lateral and longitudinal localization in a dispersive medium," Opt. Lett. **22**, 310 (1997).
3. S. Longhi, "Localized subluminal envelope pulses in dispersive media," Opt. Lett. **29**, 147 (2004).
4. G. Pariente and F. Quéré, "Spatio-temporal light springs: extended encoding of orbital angular momentum in ultrashort pulses," Opt. Lett. **40**, 2037 (2015).
5. M. Yessenov and A. F. Abouraddy, "Accelerating and decelerating space-time optical wave packets in free space," Phys. Rev. Lett. **125**, 233901 (2020).
6. A. Chong, C. Wan, J. Chen, and Q. Zhan, "Generation of spatiotemporal optical vortices with controllable transverse orbital angular momentum," Nat. Photonics **14**, 350 (2020).
7. S. W. Hancock, S. Zahedpour, A. Goffin, and H. M. Milchberg, "Free-space propagation of spatiotemporal optical vortices," Optica **6**, 1547 (2019).
8. L. Allen, M. W. Beijersbergen, R. J. C. Spreeuw, and J. P. Woerdman, "Orbital angular momentum of light and the transformation of Laguerre-Gaussian laser modes," Phys. Rev. A **45**, 8185 (1992).
9. M. Padgett and R. Bowman, "Tweezers with a twist," Nat. Photonics **5**, 343 (2011).
10. N. Bozinovic, Y. Yue, Y. Ren, M. Tur, P. Kristensen, H. Huang, A. E. Wilner, and S. Ramachandran, "Terabit-scale orbital angular momentum mode division multiplexing in fibers," Science **340**, 1545 (2013).
11. M. Krenn, M. Malik, M. Erhard, and A. Zeilinger, "Orbital angular momentum of photons and the entanglement of Laguerre–Gaussian modes," Philos. Trans. A Math. Phys. Eng. Sci. **375**, 20150442 (2017).
12. A. M. Yao and M. J. Padgett, "Orbital angular momentum: origins, behavior and applications," Adv. Opt. Photon. **3**, 161 (2011).
13. A. P. Sukhorukov and V. V. Yangirova, "Spatio-temporal vortices: properties, generation and recording," Proc. SPIE **5949**, 594906 (2005).

14. K. Y. Bliokh and F. Nori, "Spatiotemporal vortex beams and angular momentum," Phys. Rev. A **86**, 033824 (2012).
15. N. Jhajj, I. Larkin, E. W. Rosenthal, S. Zahedpour, J. K. Wahlstrand, and H. M. Milchberg, "Spatiotemporal optical vortices," Phys. Rev. X **6**, 031037 (2016).
16. S. W. Hancock, S. Zahedpour, and H. M. Milchberg, "Mode structure and orbital angular momentum of spatiotemporal optical vortex pulses," Phys. Rev. Lett. **127**, 193901 (2021).
17. S. Huang, P. Wang, X. Shen, and J. Liu, "Properties of the generation and propagation of spatiotemporal optical vortices," Opt. Express **29**, 26995 (2021).
18. S. W. Hancock, S. Zahedpour, and H. M. Milchberg, "Second-harmonic generation of spatiotemporal optical vortices and conservation of orbital angular momentum," Optica **8**, 594 (2021).
19. Y. Fang, S. Lu, and Y. Liu, "Controlling photon transverse orbital angular momentum in high harmonic generation," Phys. Rev. Lett. **127**, 273901 (2021).
20. Q. Cao, J. Chen, K. Lu, C. Wan, A. Chong, and Q. Zhan, "Non-spreading Bessel spatiotemporal optical vortices," Sci. Bull. **67**, 133 (2022).
21. W. Chen, W. Zhang, Y. Liu, F. C. Meng, J. M. Dudley, and Y. Q. Lu, "Time diffraction-free transverse orbital angular momentum beams," Nat. Commun. **13**, 4021 (2022).
22. A. Mirando, Y. Zang, Q. Zhan, and A. Chong, "Generation of spatiotemporal optical vortices with partial temporal coherence," Opt. Express **29**, 30426 (2021).
23. S. W. Hancock, S. Zahedpour, and H. M. Milchberg, "Transient-grating single-shot supercontinuum spectral interferometry (TG-SSSI)," Opt. Lett. **46**, 1013 (2021).
24. S. Huang, P. Wang, X. Shen, J. Liu, and R. Li, "Diffraction properties of light with transverse orbital angular momentum," Optica **9**, 469 (2022).
25. G. Gui, N. J. Brooks, B. Wang, H. C. Kapteyn, M. M. Murnane, and C. T. Liao, "Single-frame characterization of ultrafast pulses with spatiotemporal orbital angular momentum," ACS Photonics **9**, 2802 (2022).
26. J. Huang, J. Zhang, T. Zhu, and Z. Ruan, "Spatiotemporal differentiators generating optical vortices with transverse orbital angular momentum and detecting sharp change of pulse envelope," Laser Photonics Rev. **16**, 2100357 (2022).
27. C. Wan, Q. Cao, J. Chen, A. Chong, and Q. Zhan, "Toroidal vortices of light," Nat. Photonics **16**, 519 (2022).
28. C. Wan, J. Chen, A. Chong, and Q. Zhan, "Generation of ultrafast spatiotemporal wave packet embedded with time-varying orbital angular momentum," Sci. Bull. **65**, 1334 (2020).
29. C. Wan, J. Chen, A. Chong, and Q. Zhan, "Photonic orbital angular momentum with controllable orientation," Natl. Sci. Rev. **9**, nwab149 (2022).
30. J. Chen, P. Zheng, and Q. Zhan, "Towards optical toroidal wavepackets through tight focusing of the cylindrical vector two dimensional spatiotemporal optical vortex," Opt. Express **30**, 46666 (2022).
31. A. Lotti, A. Couairon, D. Faccio, and P. Di Trapani, "Energy-flux characterization of conical and space-time coupled wave packets," Phys. Rev. A **81**, 023810 (2010).